J. Micropalaeontology, 43, 269–282, 2024
https://doi.org/10.5194/jm-43-269-2024

Journal of Micropalaeontology
Open Access

Direct link between iceberg melt and diatom productivity demonstrated in Mid-Pliocene Amundsen Sea interglacial sediments

Heather Furlong and Reed Paul Scherer

Department of Earth, Atmosphere and Environment, Northern Illinois University, DeKalb, IL, 60115, USA

Correspondence: Heather Furlong (heatherfurlong4@gmail.com)

Received: 27 October 2023 – Revised: 4 June 2024 – Accepted: 18 June 2024 – Published: 1 August 2024

Abstract. Iceberg influence on diatom productivity has been observed for the present and suggested for the past, but direct seeding of the Southern Ocean during times of ice sheet collapse has never been directly demonstrated. Here we demonstrate enhanced diatom production and accumulation in the Amundsen Sea during a Mid-Pliocene interglacial that precisely coincides with pulses of ice-rafted debris (IRD) accumulation, and we infer a causal relation. International Ocean Discovery Program (IODP) Expedition 379 obtained continuous sediment records from the Amundsen Sea continental rise to document West Antarctic Ice Sheet (WAIS) history in an area currently experiencing the largest ice loss in Antarctica. Scanning electron microscopy (SEM) imagery of Mid-Pliocene interglacial sediments of Marine Isotope Stage (MIS) (GI-17, $\sim$3.9 Ma) documents distinct intervals of IRD-rich diatomite, whereas the overall diatom abundance and concentration of bloom species is relatively low in the absence of visible IRD. Sand- and granule-sized IRD grains are documented fully encased within diatomite laminae, with some displaying soft-sediment micro-deformation formed by grains falling into soft diatom ooze. IRD-rich diatomite layers are often characterized by nearly monospecific assemblages of the pelagic diatom *Thalassiothrix antarctica*, indicating very high primary productivity as IRD grains fell. Diatom-filled fecal pellets with clusters of barite grains are also documented within some of these laminae, further indicating direct mass sinking of diatom mats. Melting icebergs release soluble nutrients along with IRD; thus the coincidence of IRD and bloom species in Amundsen Sea sediments provides compelling evidence that iceberg discharge and melting directly initiates enhanced diatom productivity in the Southern Ocean. These results may contribute to interpreting past WAIS history by providing another proxy for potential collapse events. Furthermore, we suggest that ice sheet collapse may more broadly enhance Southern Ocean diatom production, which in itself can contribute to increased carbon export, potentially attenuating or countering the warming that may have triggered the collapse.

1 Introduction

Anthropogenically induced climate change in the polar regions is a global issue especially relevant to low-lying coastal communities, which are most vulnerable to direct and indirect effects of sea-level rise. Over the past 60 years, annual atmospheric carbon dioxide levels have been increasing at a rate nearly 100 times faster than previous natural increases (Lan et al., 2020). Consequently, the future of the Antarctic ice sheets, specifically the West Antarctic Ice Sheet (WAIS), is of significant concern due to its bed topography; its history of past collapse (Scherer et al., 1998; Naish et al., 2009; Mercer, 1978); and the observed ongoing ice loss, especially in the Amundsen Sea sector (Rignot et al., 2019). Recent research has shown that the rising sea surface temperatures and enhanced advection of warm Modified Circumpolar Deep Water (MCDW) toward the ice margin, driven in part by increasing offshore surface winds (Morlighem et al., 2020), may cause melting under ice shelves and grounding line retreat, accelerating iceberg calving (Rignot et al., 2019; Greene et al., 2022). It has even been suggested that a tipping point may already have been reached (Bett et al., 2024).

Previous WAIS studies that utilized microfossils, such as diatoms, have found evidence that the past collapse of the ice sheet in the Amundsen Sea sector may have occurred during some Pleistocene interglacials (Konfirst et al., 2012; Hillenbrand et al., 2009). The ANDRILL Project (AND-1B) provided evidence of obliquity-paced ice sheet oscillations that likely included complete WAIS collapses through much of the Pliocene in the Ross Sea sector (Naish et al., 2009; Pollard and DeConto 2009). However, the frequency, speed, and precise timing of collapse events remain uncertain (Scherer et al., 1998; Pollard and DeConto, 2009; DeConto and Pollard, 2016; McKay et al., 2012). Diatom assemblages are vital components of the Antarctic ecosystem and nutrient cycle, and they respond quickly to environmental changes in the surface waters. Their fossilized frustules, through morphometrics and assemblage data, are utilized as paleoclimate proxies to better understand past climatic changes (Dixit et al., 1992; Ruggiero et al., 2024). However, accumulations of marine diatom frustules in seabed sediments do not generally accurately reflect the living community in which they live because several factors that alter the assemblages between the death and deposition of the various diatom species are responsible for a modified species preservation (McMinn, 1995). These taphonomic factors include dissolution, selective predation, and bioturbation (McMinn, 1995; Warnock and Scherer, 2015b). Diatomites in sedimentary sequences correlate with high rates of primary productivity, export production, and preservation in the sediments (Warnock and Scherer, 2015b; Johnson, 1974; McMinn, 1995). However, individual diatom laminae may represent unique events resulting from storm-induced mass deposition events that may not reflect prevailing conditions over longer timescales (Leventer et al., 2002).

Evidence of diatom productivity due to iceberg seeding

Past studies have shown bioavailable iron to be a key limiting nutrient for phytoplankton growth offshore and around the Antarctic continent (Gerringa et al., 2012; Laufkötter et al., 2018). The supply of iron from (sub-)glacial sources into the Southern Ocean via iceberg calving and melting and subglacial meltwater outflow has been found to drive $\sim 30\,\%$ of the carbon export to marine sediments (Laufkötter et al., 2018; Thuróczy et al., 2012). MCDW upwelling at the Antarctic continental slope and onto the continental shelf negatively impacts grounding lines and ice shelves through the thermal erosion and undercutting of ice shelves, promoting melting below ice shelves and near the grounding line, thus enhancing iceberg calving and the delivery of continentally sourced nutrients into the Southern Ocean (Gerringa et al., 2012).

Although glacially transported, terrestrially derived iron is a major factor in Southern Ocean phytoplankton growth, as modern studies have indicated (e.g., Raiswell et al., 2008, 2016; Duprat et al., 2016; Wu and Hou, 2017; Hopwood et al., 2019), no prior study has established that the past loss of large sectors of the WAIS through iceberg discharge directly served as a catalyst for high rates of primary productivity in the Southern Ocean. However, a similar scenario was hypothesized on the basis of the expected silica supply to the Southern Ocean caused by a WAIS collapse by Pollock (1997). Enhanced primary productivity during prior interglacial periods could have significantly expanded carbon export. The polynyas of the Amundsen Sea and Pine Island Bay display some of the highest rates of primary productivity in the Southern Ocean (St-Laurent et al., 2017, 2019; Planquette et al., 2013). Although it is generally accepted that ice melt is one of the largest contributors of iron to the upper 300 m of the Amundsen Sea water column (St-Laurent et al., 2019), direct sources of iron that maintain intense seasonal phytoplankton blooms have not been specifically identified (Gerringa et al., 2012).

2 Materials and methods

2.1 Materials

IODP Expedition 379 drilled two sites on Resolution Drift on the Amundsen Sea continental rise (Gohl et al., 2021). This study focused on Site U1532 (68°36.6952′ S, 107°31.4721′ W; drilled in 3962 m of water), located on the western upper flank of Resolution Drift, about 270 km north of the Amundsen Sea Embayment continental shelf edge, which receives glaciogenic detritus from the WAIS (Fig. 1). Resolution Drift is a part of a system of five parallel sediment drifts on the rise and is characterized by gentle western flanks but steep eastern flanks (Horrocks, 2018). Site U1532 contains no apparent unconformities and consists of silty clay with dispersed sand and gravel and variable biogenic content (mostly diatoms). Six lithofacies were identified, with the dominant lithofacies assemblages being planar thinly laminated silty clay, generally interpreted as forming during glacial periods, with thinner occurrences of massive or bioturbated silty clay, commonly diatomaceous, interpreted as interglacials (Gohl et al., 2021). Dispersed sand grains, granules, and occasional pebbles, interpreted as ice-rafted detritus (IRD), are notable in the interglacial deposits. An apparent correlation between diatomaceous sediments and pulses of IRD was noted during the expedition (Gohl et al., 2021). Here we focus on an interglacial interval in U1532C-6F, Sections 1 and 2, which has been dated to the Mid-Pliocene Marine Isotope Stage GI-17 interglacial, near the end of the Gilbert chron (~ 3.9 Ma) (Gohl et al., 2021).

2.2 Analytical methods and procedures

Subsampling of U1532C-6F utilized a new technique developed for the project, whereby 5 mm deep V-channel samples were cut from the core surface and placed in aluminum carriers with three 10 cm long V-shaped troughs (Fig. 2).

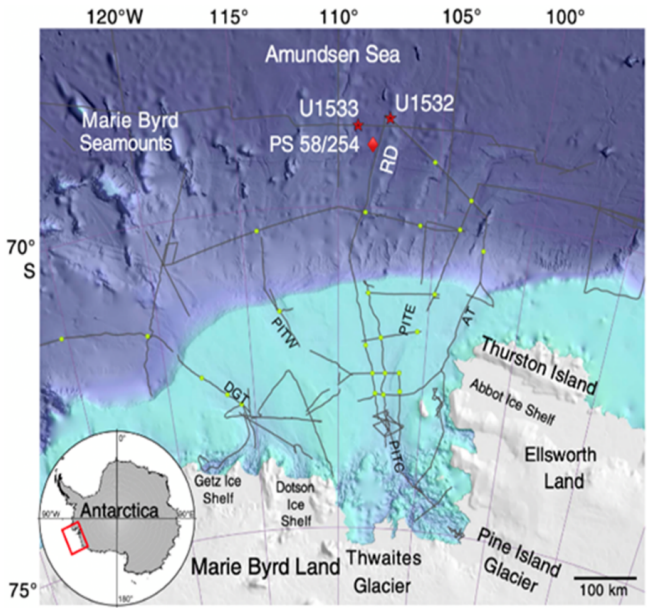

Figure 1. Location map of IODP Expedition 379 sites U1532 and U1533 (Gohl et al., 2019). Also noted is piston core PS 58/254.

The purpose of this sampling method was to preserve in situ microstratigraphy of the cores for analysis. This new sampling technique allows appropriately sized carriers, or trays, to be directly placed in the low-vacuum scanning electron microscope. This sampling was completed before all other subsampling of the core, but the shallow V-channel depth preserves the integrity of the main sample half for other analyses (Fig. 3).

Following sampling, each tray was imaged using a Leica M80 stereo zoom microscope at 12.5× magnification. The photos were taken in 1 cm by 1 cm increments and digitally stitched to create a continuous high-resolution picture of the channels (Fig. 4).

Specific strategies for targeted microstratigraphic subsampling analysis using SEM and energy-dispersive X-ray spectroscopy (EDS) with elemental mapping capability were guided by the initial optical analyses illustrated in Fig. 4. Additionally, these images were used to map IRD concentration, size, orientation, and relative abundance. Larger IRD clusters are defined as clasts > 0.5 cm, and smaller IRD clusters are defined as visible sand grains < 0.5 cm. All intervals, including those with and without IRD, are labeled with the corresponding tray number and channel letter, as well as the composite depth. Continuous low-vacuum SEM analysis was used to document microstratigraphy and analyze the sedimentary fabric of the diatomaceous sediments and to detect the presence of coincident sand- and granule-sized IRD. IRD grains were investigated for coincident winnowing or sorting and for evidence of in situ soft-sediment micro-deformation. EDS mapping was performed to analyze the chemical composition of IRD grains and to map the occurrence and distribution of trace elements, including barium. Authigenic barite crystals in marine sediments have been shown to provide a proxy for primary productivity (Bonn et al., 1998; Carter et al., 2020) whereby the crystals form as organic matter decays.

The method of Warnock and Scherer (2015a) was used to determine the absolute abundance of diatoms (ADA) within the sediment in valves per gram (vpg) dry sediment from discreet samples. A freeze-dried sample mass of ~ 0.02 g was used in intervals with high diatom abundance. This small sample size allowed the careful targeting of sub-millimeter-thick diatomite laminae and of bioturbated units. Diatom counts were performed at 1000× magnification, using a Leica DMLB reflected light microscope, to calculate the abundance of whole diatom valves, following standardized procedures. In conjunction with ADA, the percentage of biogenic silica (BSi) was determined using an adapted version of the Mortlock and Froelich (1989) method, which is outlined in the Supplement. Following dissolution steps, a UV–Vis spectrophotometer was used to measure the absorbance of the samples to calculate the percentage of opal. To document diatom assemblages within the sample intervals studied, a relative abundance approach was used to track paleoenvironmental changes. A total of 42 slides were analyzed through the studied interval, and between 300–400 individual diatoms were counted for statistically significant assemblage results. Following standard counting techniques, all diatoms had to be over 50 % intact in order to be tallied. The diatoms within the *Thalassiothrix* group were rarely intact, and, as a result, only terminal ends of the valves were counted, then the total number of individuals found was divided by 2 to account for the valves on each end of the individual diatom valves. Valves of *Dactyliosolen antarctica* are rarely preserved, but girdle bands are prominent and distinctive, resulting in an overcount that cannot be precisely corrected for because each cell contains a variable abundance of girdles. Diatoms were split into respective species groups, and the percentages of diatoms were calculated to compare relative abundances from each depth interval.

3 Results

3.1 Light microscopy imaging and scanning electron microscopy

Light microscopy imaging allowed several IRD events to be identified throughout the 2 m section from 197.26 to 199.5 m b.s.f. IRD intervals with large clasts, and clusters of smaller clasts were identified through visual inspection, denoted, and further studied for signs of increased primary productivity surrounding the clasts under low-vacuum SEM (Fig. 4). All primary indications of diatomite layers and bioturbation were also recorded. Large IRD clasts occur in Tray 1 Channel B (197.403 m), Tray 1 Chan-

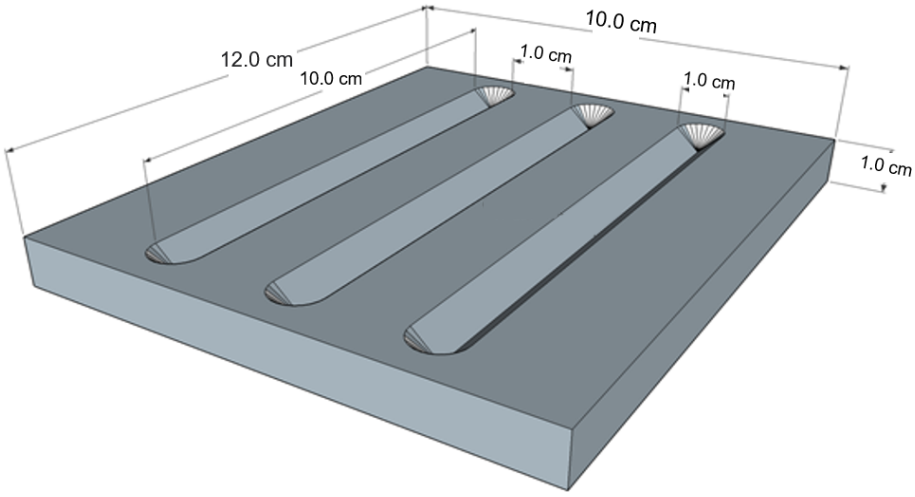

Figure 2. Rendering of V-channel aluminum carriers.

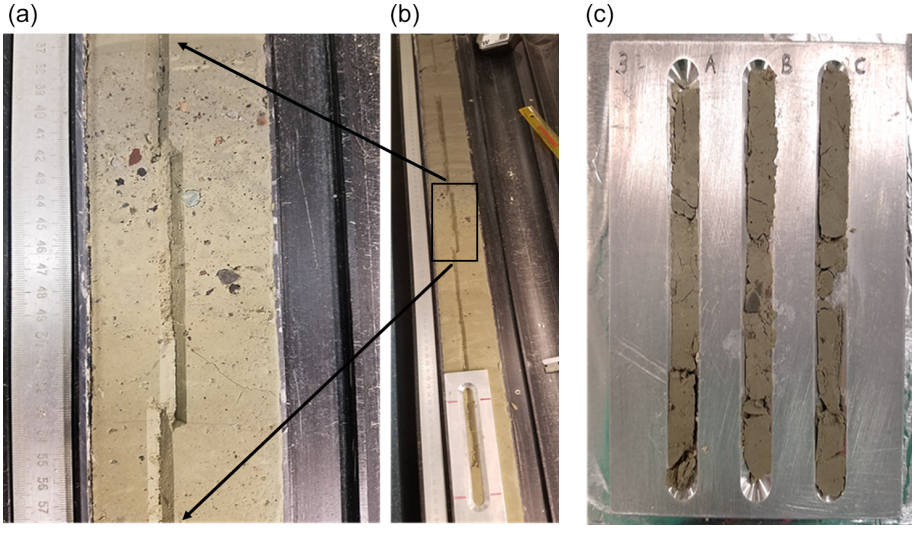

Figure 3. Panels **(a)** and **(b)** illustrate how the V-channel samples were collected from the core using a minimally invasive and low-disturbance technique that allows later sampling of the same area for other scientific analyses. The bottom of panel **(b)** shows the cutting guide used to obtain a precise 45° angle. Panel **(c)** shows filled Tray 3 (197.8–198.1 m b.s.f.).

nel C (197.542 m, 197.577 m, 197.578 m, and 197.596 m), and Tray 2 Channel C (197.846 m). Numerous clusters of small IRD clasts were found sporadically throughout the core from Tray 1 Channel A (197.318 m) to Tray 6 Channel B (198.974 m). Low-vacuum SEM imagery enabled a preliminary assessment of diatom species within the sample and of the approximate locations of larger IRD clasts and smaller IRD clusters (Fig. 5). SEM images also captured instances of soft-sediment micro-deformation associated with dropstones coincidentally falling and becoming encapsulated into diatomaceous ooze laminae.

3.2 Absolute diatom abundance and biogenic silica

Overall, ADA at Site U1532C-6F alternated between intervals of high diatom accumulation and sections that had low abundance or were entirely barren. The highest diatom abundance is $> 3 \times 10^7$ valves per gram (vpg) dry sediment, with average peaks occurring between 2×10^7 and 2.5×10^7 vpg and low-abundance intervals ranging from 0 to 1×10^7 vpg. Diatom abundance drops toward barren in the laminated silts that overlie the IRD-rich diatomite, but the base of the silty laminae contains abundant highly fragmented and size-sorted diatoms with no coarse detrital grains, indicating transport and sorting by bottom currents. The absence of a lag of coarser sediments at the contact suggests that the contact is likely conformable, not significantly erosional.

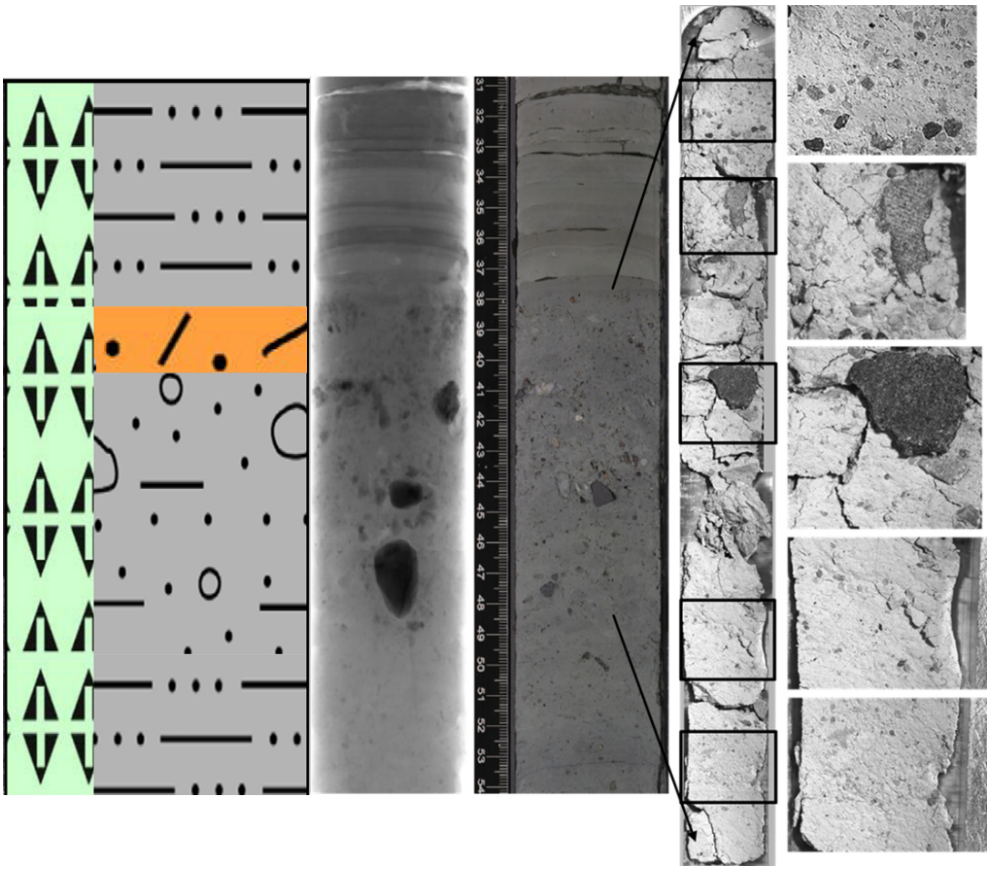

Figure 4. Subunit IB, shown with facies F2.1 (31–38 cm), F4 (39–50 cm), and F3 (50–54 cm), adapted from Gohl et al. (2021). The image on the left is the graphic lithology from Gohl et al. (2021), displaying the biosilica-rich sandy mud with dispersed clasts that transitions to a clast-rich muddy diamict, followed by clast-free laminated sorted silts at the top. The X-radiograph (center-left image) shows several large IRD clasts that are not visible in the photo from the split-core surface (center-right image) The V-channel composite core image on the right is composed of 14 1 cm by 1 cm individual images taken from core section U1532C-6F-1, Tray 2 Channel A (197.53–197.63 m b.s.f.), where two large IRD clasts and numerous smaller IRD clusters are observed. Close-ups of this composite image (marked by black rectangles) are presented in the panel to the right.

The overlying laminated silts have been interpreted as resulting from glacial advance and gravitational transport of glaciogenic detritus down the continental slope, with rapid emplacement of its fine-grained components on the rise that characterizes much of Resolution Drift (Gohl et al., 2021). Along with ADA, biogenic silica (BSi) concentrations at Site U1532C-6F alternated between intervals of high to extremely low percentages (Fig. 6). The highest concentration is 42 wt % at 198.12 m, with averages of about 13 wt %. Low-concentration intervals contain less than 5 wt % BSi, with the lowest BSi concentration being 1.74 wt % at 199.185 m. Maximum BSi percentages, along with high pelagic diatom abundance, occur in distinct horizons together with high IRD concentrations (shaded areas in Fig. 6) within the upper part of the studied interval. This indicates that the accumulation rate of IRD within these horizons was high because the deposition of the diatom-rich sediments can be expected to have taken place rapidly.

3.3 Diatom species assemblages

Throughout the entire studied core interval, more than 40 different Southern Ocean diatom species were identified. The species with the highest concentrations are *Dactyliosolen antarcticus* intercalary bands, which on average comprised 14.4 % of all diatoms counted. However, *D. antarcticus* percentages are not based on counts of whole valves, and each cell may contain dozens of robust bands. Consequently, high *D. antarcticus* percentages significantly overestimate actual valve abundance. In whole valve counts, the most abundant species was *Thalassiothrix* (*Tx.*) *antarctica*, which had an average percentage of 10.6 % (corrected for tip counts), followed by *Fragilariopsis barronii* with an average of 10.1 %. Figure 7 displays the most prevalent diatom genera found within the sampled interval. However, certain laminae not directly represented in quantitative counts but observed in the SEM analysis contain a nearly monospecific assemblage of *Tx. antarctica*.

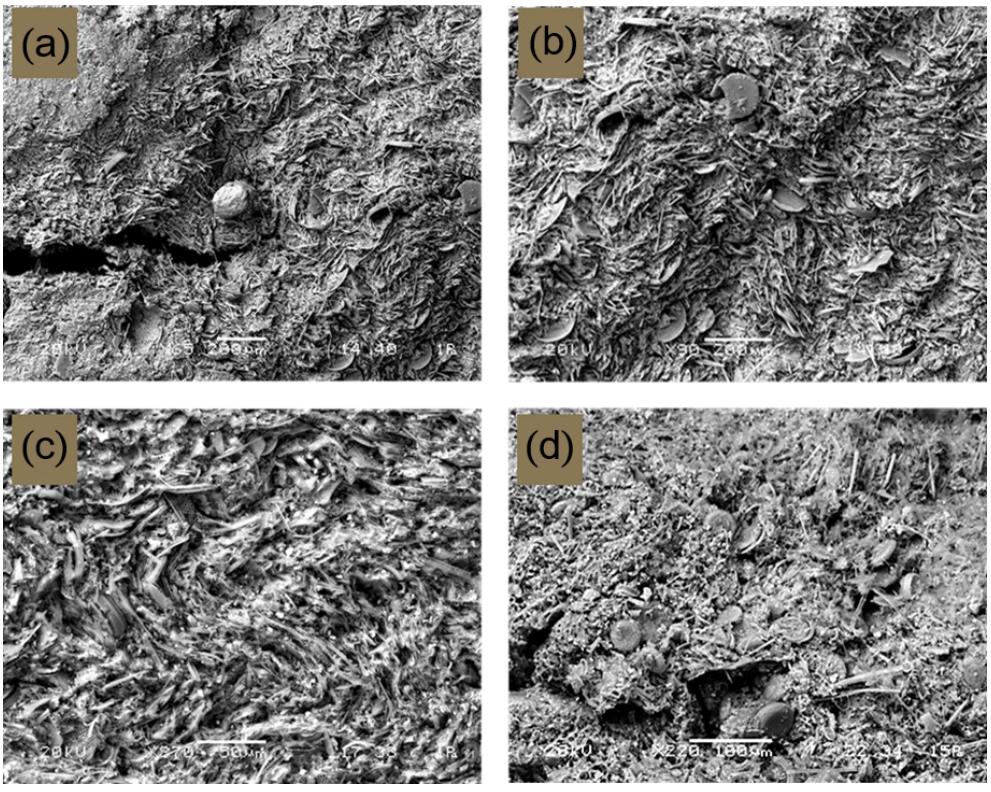

Figure 5. **(a)** Tray 4 Channel B (198.346 m) shows a dropstone encapsulated by mostly *Tx. antarctica* and a few centric species. **(b)** Tray 4 Channel B (198.383 m) shows a concentrated mat of mostly *Tx. antarctica* and several centric species including *T. inura* and *T. complicata*. **(c)** Tray 3 Channel C (198.134 m) shows a concentrated mat of nearly all *Tx. antarctica*. **(d)** Tray 3 Channel A (197.946 m) shows a disorganized layer containing a large concentration of *Tx. antarctica*, *Tx. longissima*, *Trichotoxon reinboldii*, and several *Thalassiosira* species.

The *Fragilariopsis* group of pennate diatoms made up a large portion of the species within the upper part of the studied interval. *F. barronii* preferred cooler Antarctic environments, 0–8 °C, which prevail in the Antarctic Zone (AZ) and the Polar Front Zone (PFZ) of the modern Southern Ocean (Abelmann et al., 1990; Dowsett et al., 1996; Zielinski and Gersonde, 1997). The species *F. separanda*, which is present in modern southern cold open-water regions (Cefarelli at al., 2010), had a very low abundance in the Mid-Pliocene interval from Site U1532. Other cold water indicating *Fragilariopsis* species such as *F. aurica* and *F. arcula*, which both have Late Miocene first occurrences (Censarek and Gersonde, 2002), occurs in this interval. *F. curta* and closely related taxa, indicative of seasonal winter sea ice (Crosta et al., 2008), are also present in very low abundance. The *Thalassiosira* group is one of the most commonly occurring centric diatom groups present throughout the interval. *Thalassiosira* species consistent with an early to middle Pliocene age found in the studied samples include *T. complicata*, *T. fasciculata*, *T. inura*, *T. kolbei*, *T. lentiginosa*, *T. oliverana*, *T. praelineata*, *T. striata*, and *T. tumida*. The *Rouxia* group is consistently present throughout this entire interval. The species *R. constricta*, which represents relatively cold-water conditions (Zielinski et al., 2002), occurs sparsely throughout. *R. antarctica*, also present throughout the entire interval, is a middle to late Pliocene species suggested to be indicative of surface water stratification due to seasonal meltwater (Armbrecht et al., 2018). The occurrence of *R. naviculoides* within the U1532 interval is also suggestive of stratification associated with seasonal meltwater (Armbrecht et al., 2018).

4 Discussion

4.1 Scanning electron microscopy

Low-vacuum SEM imagery captured instances of soft-sediment micro-deformation associated with dropstones falling into accumulating diatomaceous ooze, with several examples illustrated from U1532C-6F-1-110/111cm, at approximately 198.2 m b.s.f. (Fig. 8). Figure 8a shows the outline of a diatomaceous ooze layer with a fully encapsulated dropstone. Figure 8b shows the transition from terrigenous silt-rich sediment to almost pure diatomite composed of a nearly monospecific assemblage of the pelagic diatom *Tx. antarctica*. This pelagic species is known to thrive under high nutrient availability (Kemp et al., 2000, 2010). Dur-

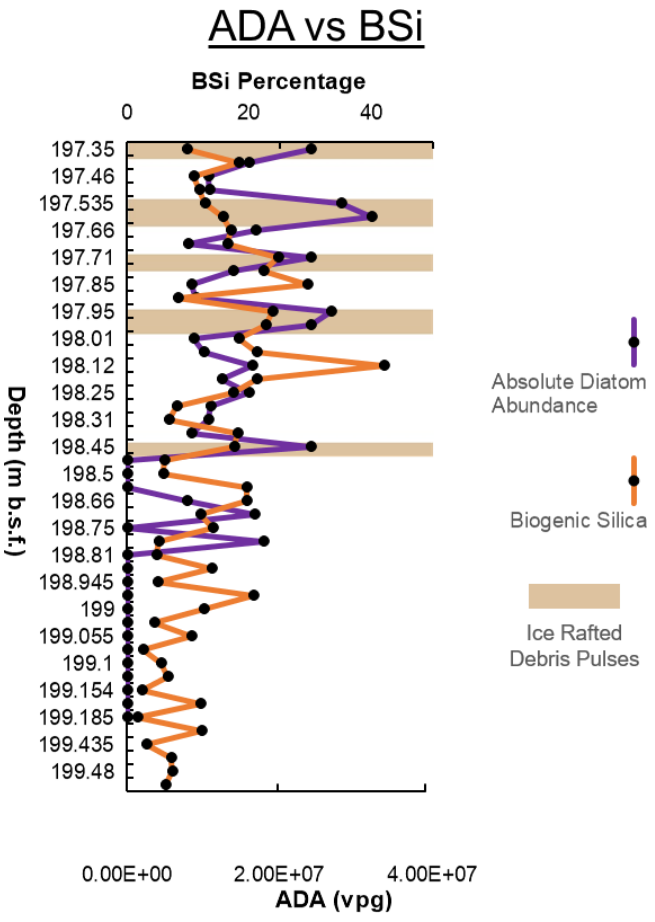

Figure 6. Absolute diatom abundance (ADA) in valves per gram (vpg) and biogenic silica (BSi) content plotted against depth. ADA is much higher near the top of the studied interval and approaches zero in the lowermost ca. 0.5 m. The horizons with higher ADA near the top of the interval correlate with high IRD concentrations, indicated by the shaded brown boxes, despite the fact that IRD represents terrigenous dilution of the diatoms. Generally, high percentages of BSi are found in the upper part of the studied interval, and they are lowest in the lowest part of the interglacial.

ing blooms, frustules can become entangled and interlocked, forming mats that rapidly sink en masse through the water column down to the seafloor, thus potentially representing a single instantaneous event or repeated instantaneous events in the sedimentary record. The corresponding layers in U1532 also contain abundant authigenic barite crystals (Fig. 8c), which are known to develop in decaying organic matter in the water column (e.g., Paytan and Griffith, 2007); thus high concentrations of authigenic barite crystals have been used as a paleoproductivity indicator (e.g., Bonn et al., 1998; Liguori et al., 2016). Individual *Tx. antarctica* laminae could have formed in a single season, with sinking of a bloom-induced mat, but more continuous laminae (less than 0.25 cm thick) typically represent repeated seasons of high primary productivity. Collectively, these observations demonstrate contemporaneousness of enhanced diatom and IRD deposition, thus confirming the link between iceberg melt and high primary productivity over repeated seasons, likely spanning decades to centuries. We note that the IRD grains themselves would not be the nutrient source, but melting icebergs also release much finer particles along with soluble and microparticulate iron and other nutrients. Figure 8d shows an inferred plankton fecal pellet, displaying a concentrated cluster of barite microcrystals, noted in EDS elemental scanning. A cluster of authigenic barite in these pellets further implies high productivity with rapid deposition. The stratigraphic occurrence of these barite-rich fecal pellets with IRD further links high primary productivity with increasing iceberg melt.

Figure 9 shows the core image of Core Section U1532C 6F-1 from 110–140 cm (198.2 to 198.5 m b.s.f.) on the left, with close-up photos shown to the right. The SEM close-up image from 130.5–131.0 cm (198.410 m b.s.f.) on the right captures a diatomaceous sediment ooze layer comprised almost entirely of *Tx. antarctica*. The image on the top right shows another encapsulated dropstone at 50× magnification, circled in white, also surrounded by *Tx. antarctica*.

Figure 10 shows a split-core photo of U1532C6F-2 with 10 to 60 cm (198.7 to 199.2 m b.s.f.) (middle panel) and close-ups from this interval (left panel). This section was heavily bioturbated and contained well-preserved diatoms. The top image on the left shows two different centric species and a needle-like species, possibly *Tx. antarctica*, within a sediment layer. The middle and lower images in the left panel display a pocket of mixed pelagic diatom species within a diatom-rich sediment layer (indicated by the circle in the lower image). There are several examples of encapsulated dropstones within this section as well. A mixed species assemblage in bioturbated diatomite reflects slower overall sediment accumulation rates than monospecific diatomaceous ooze laminae. The image in Fig. 10 suggests that this section was characterized by a gradual transition from glacial silt and clay sedimentation to bioturbated sediment with modest diatom abundance, followed by rapid, enhanced IRD and diatomite deposition late in the interglacial. Such conditions in the presence of common IRD, as displayed in this section, suggest persistent seasonal diatom deposition in the presence of abundant icebergs, rather than a single iceberg-melting event. This may indicate a steady release of icebergs from the WAIS into the Amundsen Sea over decades or centuries, possibly as part of a broader collapse event. Subsequent to the IRD pulse came a rapid onset of laminated glacial silt and clay deposition (marked by a sharp boundary at 197.53 m) which persisted for tens of meters. This contact represents the transition from the interglacial diatom and IRD-rich sediments to laminated diatom and IRD-poor silts, representing the rapid onset of terrigenous input and downslope transport associated with glacial readvance (Gohl et al., 2021).

A similar depositional scenario to the one described here is noted in an earlier interglacial sequence (U1533B-14H-

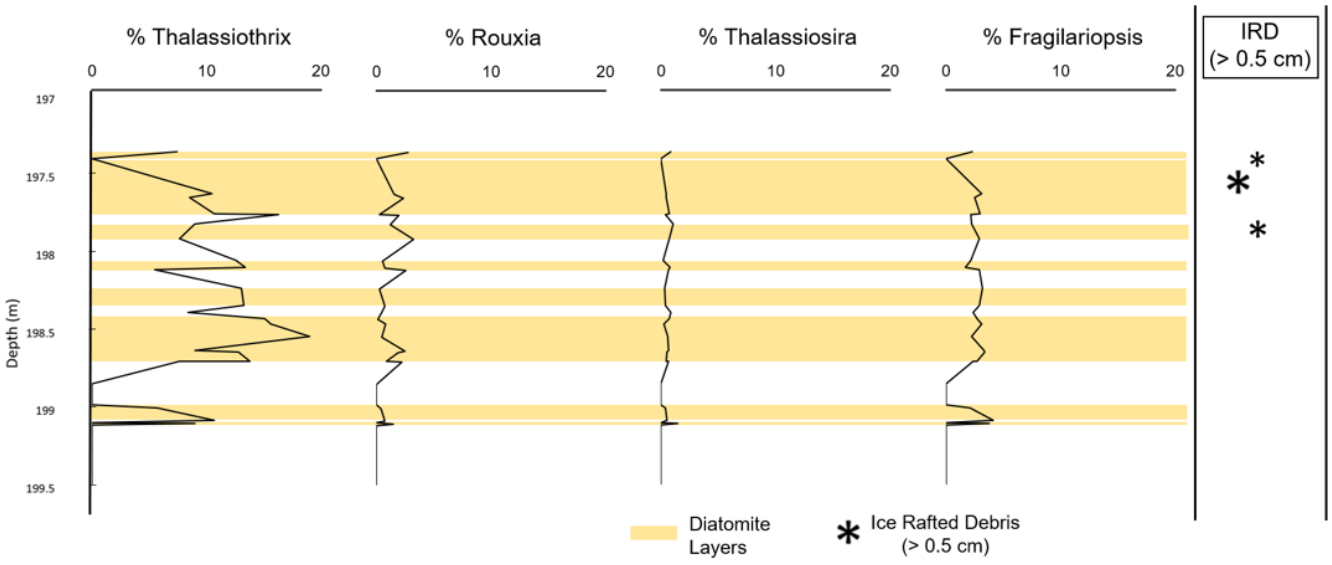

Figure 7. The most prevalent genera found within the studied interval from Site U1532 were *Thalassiothrix, Rouxia, Thalassiosira*, and *Fragilariopsis*. Asterisks indicate positions of larger IRD clasts (> 0.5 cm) in the split-core photos (Gohl et al., 2021); however, more IRD clasts (> 0.5 cm) and layers are observed in the X-ray. The size of each asterisk is proportional to the thickness of the IRD layer. Yellow bars show where diatomite layers are located.

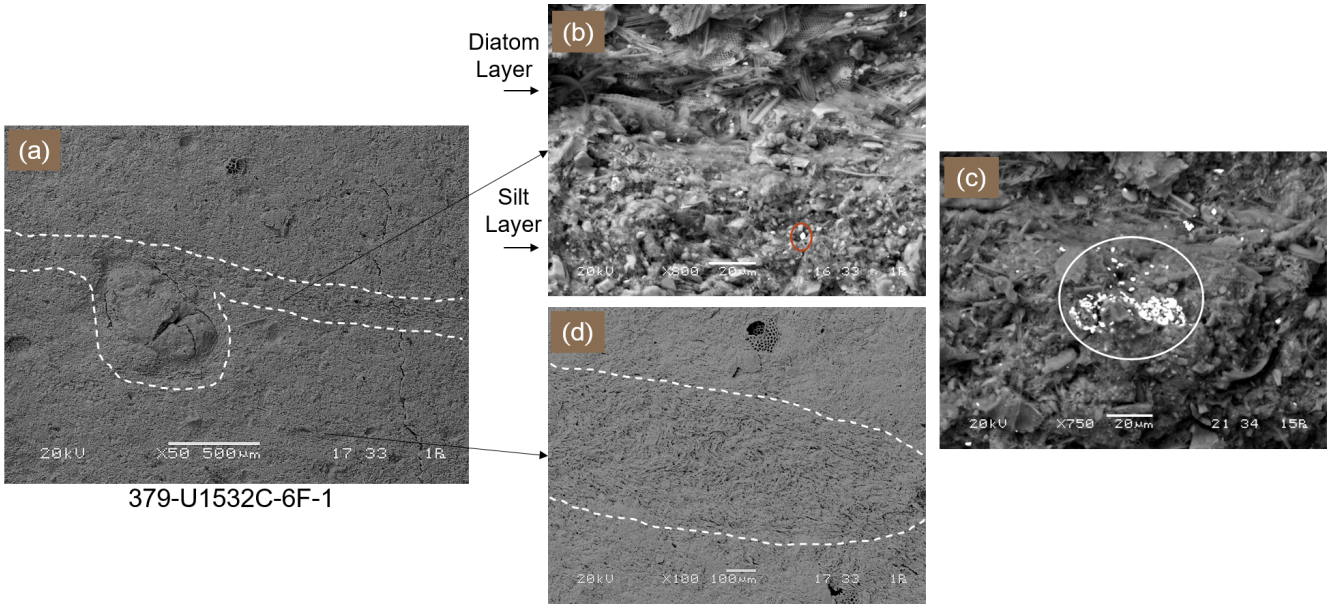

Figure 8. Images from 198.2 m b.s.f. at Site U1532. **(a)** SEM image of a till pellet dropstone completely encapsulated within a diatomaceous ooze layer, demonstrating coincidence of diatomaceous ooze deposition and soft-sediment deformation from the dropstone settling onto the seafloor. The dotted line outlines the top and bottom of this lamina. **(b)** Sharp boundary between terrigenous fine-grained sediment (below) and a nearly pure diatomite mat (above). A complete barite crystal is circled (in red). **(c)** A large concentration of authigenic barite crystals (bright spots) found within this diatomite layer, indicating high rates of primary productivity and export. **(d)** Plankton fecal pellet (outlined by a dashed white line) overlying a silty layer.

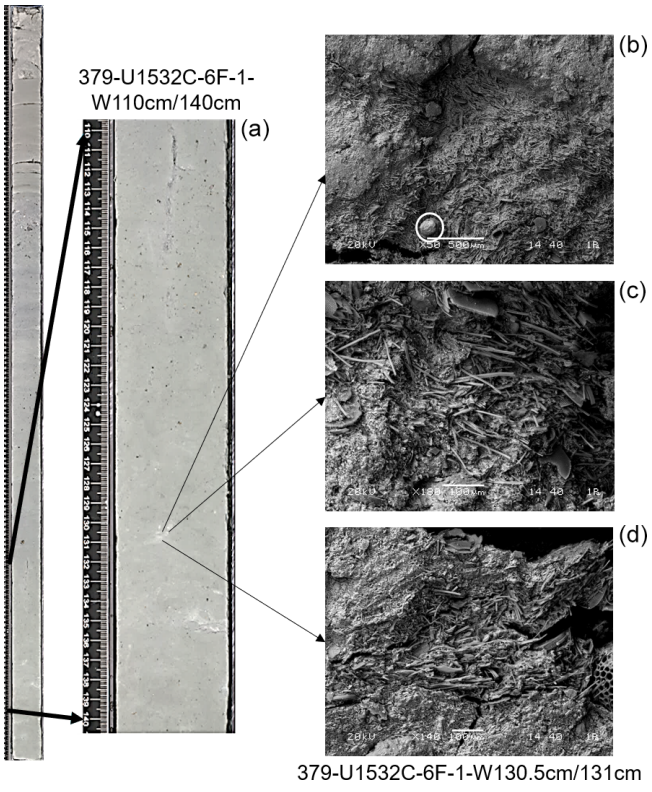

Figure 9. Split-core photo of U1532C-6F-1 with an enlarged interval from 110 to 140 cm (198.2–198.5 m b.s.f.) **(a)** and close-ups from this interval **(b–d)**. Panel **(b)** shows a dropstone encased in a diatomite layer rich in *Tx. antarctica*. Panels **(c)** and **(d)** show oriented *Tx. antarctica* and other centric species. These mat deposits of *Tx. antarctica* reflect a mass sinking event and rapid deposition of the resulting diatomaceous mats on the seafloor (Grigorov et al., 2002; Kemp et al., 2006, 2010).

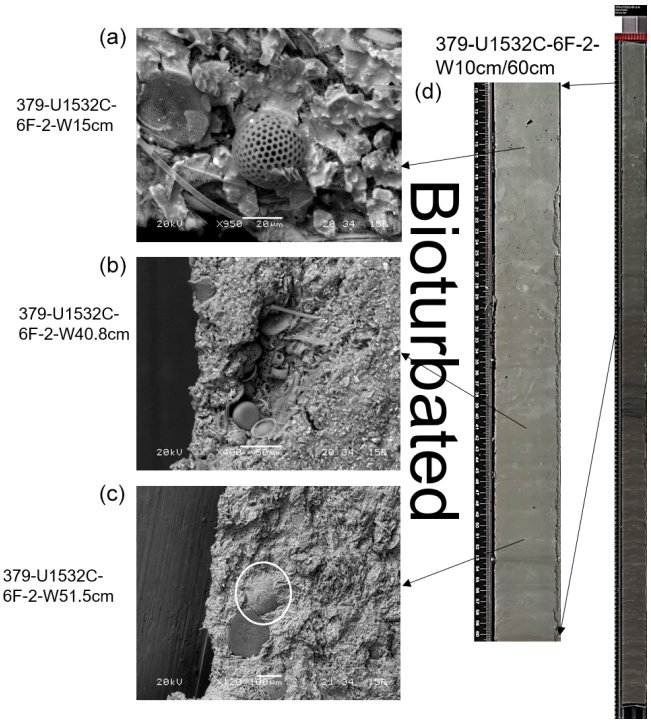

Figure 10. Split-core photo of Site U1532C-6F-2 with an enlarged interval from 10 to 60 cm (198.7 to 199.2 m b.s.f.) **(d)** and SEM images from this interval **(a–c)**. This section is heavily bioturbated, contains extensive mixed pelagic diatom species, and includes a dropstone encapsulated within diatom-rich sediment layers with mixed diatom assemblages. Overall diatom concentration (ADA) is lower in these bioturbated sediment intervals from early in the interglacial than in the more IRD-rich diatomite layers of the late interglacial interval.

1; Fig. 11). This sequence was deposited ∼ 4.5 Ma and lies 140.24 m b.s.f. (Gohl et al., 2021). Older but less deeply buried than U1532C-6F, it also contains IRD-rich interglacial diatomite and mudstone, rapidly transitioning to glacial laminated silts. This transition is abrupt, potentially indicating scour. The observations and analyses reported here for U1532C-6F cannot be directly replicated in this interval because the diatoms in U1533B-14H are diagenetically altered. Despite this limitation, the lithostratigraphic similarity suggests that the scenario described for U1532C-6F-1 is not unique.

4.2 Absolute diatom abundance and percent biogenic silica

In the Southern Ocean, diatoms are the primary contributors to the production of BSi, and the relative abundance of specific diatom taxa affects BSi accumulation in the seabed sediment (e.g., Cortese and Gersonde, 2008). We find a correlation between the percentage of BSi and ADA but also, more importantly, a strong correlation between high ADA and IRD concentrations in the studied Mid-Pliocene sediments from Site U1532, despite the fact that the rapid deposition of diatom ooze should dilute a persistent but relatively slow rain of IRD to the seafloor. This correlation suggests a causal relationship between diatom and IRD input, with high diatom abundance resulting from iceberg-derived nutrients released into the surface waters of the Amundsen Sea (Fig. 6).

The complex and pulsed IRD peaks and coinciding maxima in ADA concentrations occur only within particular diatomite horizons within the studied interval. Within an interglacial sediment horizon with very little IRD, areas of intense bioturbation are likely indicative of a lower sediment accumulation rate. Shipboard investigations revealed that quartz grains from smaller peaks in IRD concentration in a sample taken just below the interval studied here show micro-texture evidence of meltwater transport, whereas the micro-texture of quartz grains in a sample taken from an IRD peak in the middle of the studied interval revealed weathering on many of the grains (Gohl et al., 2021; Robinson et al., 2021). This may be due to a warmer ocean that influenced the melting

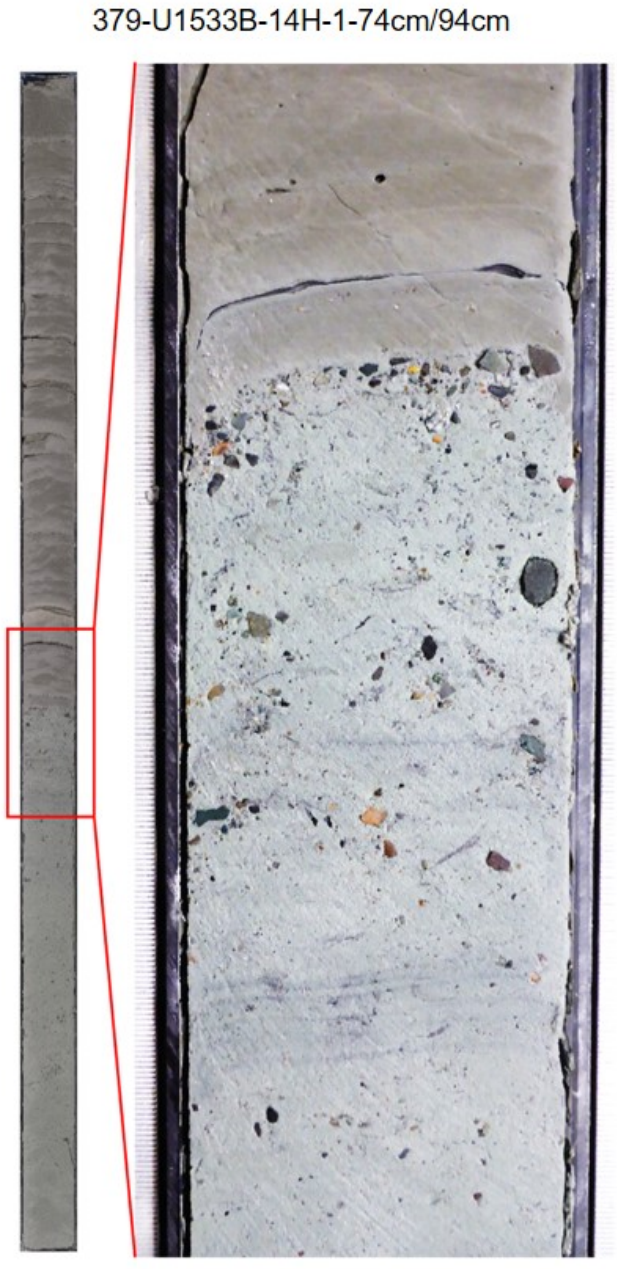

Figure 11. Core photo of a section of U1533B-14H-1 (140.24–140.44 m b.s.f.) showing correspondence of IRD and diatomite late in a Pliocene interglacial, with a sharp rapid transition, likely erosional, to overlying laminated silts. The light-colored sediments are altered diatomite. Diagenetic alteration of the diatoms precluded the detailed examination that was performed on U1532C-6F.

and distribution of the icebergs, as the more complex IRD peaks only occur in intervals with biogenic sediment. These data provide evidence of a relatively warm pelagic ocean environment in the Amundsen Sea, with primary productivity enhanced by WAIS retreat and the melting of large numbers of icebergs that were probably calved as large parts of the ice sheet decayed. The pulses of IRD supply and coinciding maxima in diatom productivity were likely caused by marine ice sheet retreat and major ice-stream drainage basin collapse, with icebergs primarily originating from the Thwaites Glacier and Pine Island Glacier basins. The described retreat events took place towards the end of the Mid-Pliocene, and they may represent the warmest phases of a sequence of warm interglacial periods that preceded a rapid return to cold glacial conditions with ice sheet readvance and reduced iceberg release.

4.3 Diatom species assemblages

During the late Pliocene to Pleistocene, *Fragilariopsis barronii*, *Actinocyclus ingens*, and species belonging to the *Thalassiothrix* group dominated diatom assemblages in the AZ and PFZ of the Southern Ocean (Cortese and Gersonde, 2008). High abundances of *Tx. antarctica*, found throughout the entire Mid-Pliocene interval from Amundsen Sea Site U1532, have been interpreted to be associated with high BSi export, burial, and efficient preservation due to the thick mats that may form in the water column (Quilty et al., 1985) and settle on the seafloor (Kemp et al., 1996). Prior work of Cortese and Gersonde (2008) indicates that mats of *Tx. antarctica* generally form in the colder areas at Southern Ocean fronts with abundant nutrients then sink en masse following resultant nutrient depletion (Kemp et al., 1996). Figures 5, 7, and 8 display visual evidence of such diatom mats in the studied sediment interval from Site U1532, indicative of their rapid deposition in the Amundsen Sea during Mid-Pliocene interglacials (Cortese et al., 2004). Other elongate araphid pennate species, including *Thalassionema nitzschioides*, *Trichotoxon reinboldii*, and *Thalassiothrix longissima*, form similar mats in warmer waters (Kopczyńska et al., 1998; Crosta et al., 2005). In the modern Southern Ocean, *Chaetoceros* resting spores, neritic high-productivity indicators (Leventer, 1991), often dominate Antarctic settings with very high primary productivity, such as the Bransfield Strait (Crosta et al., 1997). *Chaetoceros* is rare in the U1532 sediments, suggesting that the high productivity evident for interglacials from this interval were likely not triggered by coastal upwelling and shallow mixed layers typical of nearshore environments. Instead, the increase in phytoplankton productivity in the Amundsen Sea was influenced by nutrient input from extensive iceberg melting in the Amundsen Sea.

5 Conclusions

The sediments and data collected from IODP Expedition 379 provide an important snapshot of the environmental conditions during glacial and interglacial cycles of the Mid-Pliocene in this region, along with proxy details indicating WAIS collapse events through the Thwaites and Pine Island glacier corridor, notably during the interval studied here (MIS GI-17, ∼ 3.9 Ma). The content of biosiliceous material

is relatively low through many Pliocene interglacial sections at Site U1532, likely the result of diatom dissolution resulting from relatively low sediment accumulation rates. However, within several interglacial sections, clusters of IRD can be found along with very high diatom abundance. Within these intervals, the content of terrigenous fine-grained sediment components supplied by turbidity and bottom currents is low due to a rapid increase in diatom/BSi accumulation rates combined with a significantly increased flux of IRD and an absence of subglacial sediment plumes near the continental shelf edge. A causal link between iceberg melt and enhanced primary productivity is thus demonstrated. We interpret these interglacial episodes as documenting major and rapid WAIS retreat or even full collapse, with discharge of vast amounts of ice from the West Antarctic interior, largely via the Pine Island and Thwaites glacier corridors. As the large armadas of icebergs originating from the Amundsen Sea sector of the WAIS melted, they released dissolved iron and other key nutrients, together with meltwater and IRD, into the surface waters (Smith et al., 2007; Lin et al., 2001) of the Southern Ocean, triggering enhanced diatom growth and export. The extensive iceberg melting furthermore caused stratification of the upper part of the water column by freshwater (Stephenson et al., 2011; Cenedese and Straneo, 2023), which is conducive to high diatom production and carbon export. We speculate that this enhanced diatom production and carbon export may have had an impact on terminating the corresponding interglacial period and initiating the return to glacial conditions.

The Mid-Pliocene glacial–interglacial cycle of the Amundsen Sea studied here is characterized by a gradual transition from the glacial-age sedimentation of glaciogenic silt and clay to the interglacial deposition of bioturbated sediment with modest diatom abundance, followed by the rapid enhanced IRD and diatom ooze sedimentation late in the interglacial, which was subsequently rapidly terminated by the onset of renewed deposition of glacial silt and clay. These observed transitions between glacial and interglacial periods differ from the structure of typical Late Pleistocene eccentricity-paced cycles and may be characteristic of obliquity-paced climate cycles during the middle and late Pliocene. Overall, understanding the relationship between diatom productivity and IRD pulses could help to answer urgent questions about the role and internal positive and negative feedbacks of ice sheet–ocean interactions in Antarctica during a time long before humans interacted with the global climate. Establishing changes that are typical for the WAIS during times of global warming could aid international planning for a societal response to current ice sheet change and its global consequences for global sea-level rise now and for the future.

Data availability. All the data used in this study are included in the article and Supplement. Data are archived in the US Antarctic Data Center (https://www.usap-dc.org/view/dataset/601769) (Scherer, 2024). Diatom slides can be accessed at Northern Illinois University in Davis Hall room 315A.

Supplement. The supplement related to this article is available online at: https://doi.org/10.5194/jm-43-269-2024-supplement.

Author contributions. RPS collected the V-channels and described the samples at the Gulf Coast repository in College Station, Texas. The science team and technicians of IODP Expedition 379 recovered the cores. HF performed all analyses. Both authors collaborated in analyzing the results and provided input for the writing of the article.

Competing interests. The contact author has declared that neither of the authors has any competing interests.

Disclaimer. Publisher's note: Copernicus Publications remains neutral with regard to jurisdictional claims made in the text, published maps, institutional affiliations, or any other geographical representation in this paper. While Copernicus Publications makes every effort to include appropriate place names, the final responsibility lies with the authors.

Special issue statement. This article is part of the special issue "Advances in Antarctic chronology, paleoenvironment, and paleoclimate using microfossils: Results from recent coring campaigns". It is not associated with a conference.

Acknowledgements. The authors would like to thank the referees for taking the time to review the paper and for their suggestions to improve it. Additionally, we especially thank Claus-Dieter Hillenbrand for his thorough and thoughtful contributions to this work. The authors also want to thank the International Ocean Discovery Program for participation in the program and for the research and travel support. We thank the IODP Expedition 379 scientists, technicians, and crew for their many contributions. We also thank Jason Coenen, Joseph Mastro, Joseph Ruggiero, Brandon Reed, and especially Christine Siddoway for their many contributions to this research. Lastly, we thank the NIU Department of Earth, Atmosphere and Environment for providing support for conference travel to present results.

Financial support. The primary source of funds in support of this research came from NSF grant no. ANT1939139 and from the US Science Support Program for the IODP.

Review statement. This paper was edited by David Harwood and reviewed by two anonymous referees.

References

Abelmann, A., Gersonde, R., and Spiess, V.: Pliocene–Pleistocene paleoceanography in the Weddell Sea – siliceous microfossil evidence, Geological history of the polar oceans: Arctic versus Antarctic, in: Geological History of the Polar Oceans: Arctic Versus Antarctic, edited by: Bleil, U. and Thiede, J., Kluwer, Dordrecht, the Netherlands, 729–759, https://hdl.handle.net/10013/epic.10607 (last access: 29 July 2024), 1990.

Armbrecht, L. H., Lowe, V., Escutia, C., Iwai, M., McKay, R., and Armand, L. K.: Variability in diatom and silicoflagellate assemblages during mid-Pliocene glacial-interglacial cycles determined in Hole U1361A of IODP Expedition 318, Antarctic Wilkes Land Margin, Mar. Micropaleontol., 139, 28–41, https://doi.org/10.1016/j.marmicro.2017.10.008, 2018.

Bett, D. T., Bradley, A. T., Williams, C. R., Holland, P. R., Arthern, R. J., and Goldberg, D. N.: Coupled ice–ocean interactions during future retreat of West Antarctic ice streams in the Amundsen Sea sector, The Cryosphere, 18, 2653–2675, https://doi.org/10.5194/tc-18-2653-2024, 2024.

Bonn, W. J., Gingele, F. X., Grobe, H., Mackensen, A., and Fütterer, D. K.: Palaeoproductivity at the Antarctic continental margin: opal and barium records for the last 400 ka, Palaeogeogr. Palaeoecol., 139, 195–211, https://doi.org/10.1016/S0031-0182(97)00144-2, 1998.

Carter, S. C., Paytan, A., and Griffith, E. M.: Toward an improved understanding of the marine barium cycle and the application of marine barite as a paleoproductivity proxy, Minerals, 10, 421, https://doi.org/10.3390/min10050421, 2020.

Cefarelli, A. O., Ferrario, M. E., Almandoz, G. O., Atencio, A. G., Akselman, R., and Vernet, M.: Diversity of the diatom genus *Fragilariopsis* in the Argentine Sea and Antarctic waters: morphology, distribution and abundance, Polar Biol., 33, 1463–1484, https://doi.org/10.1007/s00300-010-0794-z, 2010.

Cenedese, C. and Straneo, F.: Icebergs melting, Annu. Rev. Fluid Mech., 55, 377–402, https://doi.org/10.1146/annurev-fluid-032522-100734, 2023.

Censarek, B. and Gersonde, R.: Miocene diatom biostratigraphy at ODP Sites 689, 690, 1088, 1092 (Atlantic sector of the Southern Ocean), Mar. Micropaleontol., 45, 309–356, https://doi.org/10.1016/S0377-8398(02)00034-8, 2002.

Cortese, G. and Gersonde, R.: Plio/Pleistocene changes in the main biogenic silica carrier in the Southern Ocean, Atlantic Sector, Mar. Geol., 252, 3–4, https://doi.org/10.1016/j.margeo.2008.03.015, 2008.

Cortese, G., Gersonde, R., Hillenbrand, C. D., and Kuhn, G.: Opal sedimentation shifts in the World Ocean over the last 15 Myr, Earth Planet. Sc. Lett., 224, 509–527, https://doi.org/10.1016/j.epsl.2004.05.035, 2004.

Crosta, X., Pichon, J. J., and Labracherie, M.: Distribution of Chaetoceros resting spores in modern peri-Antarctic sediments, Mar. Micropaleontol., 29, 283–299, https://doi.org/10.1016/S0377-8398(96)00033-3, 1997.

Crosta, X., Romero, O., Armand, L. K., and Pichon, J. J.: The biogeography of major diatom taxa in Southern Ocean sediments: 2. Open Ocean related species, Palaeogeogr. Palaeoecol., 223, 66–92, https://doi.org/10.1016/j.palaeo.2005.03.028, 2005.

Crosta, X., Denis, D., and Ther, O.: Sea ice seasonality during the Holocene, Adélie Land, East Antarctica, Mar. Micropaleontol., 66, 222–232, https://doi.org/10.1016/j.marmicro.2007.10.001, 2008.

DeConto, R. M. and Pollard, D.: Contribution of Antarctica to past and future sea-level rise, Nature, 531, 591–597, https://doi.org/10.1038/nature17145, 2016.

Dixit, S., Smol, J. P., Kingston, J. C., and Charles, D. F.: Diatoms-Powerful Indicators of Environmental-Change, Environ. Sci. Technol., 26, 22–33, https://doi.org/10.1021/es00025a002, 1992.

Dowsett, H., Barron, J., and Poore, R.: Middle Pliocene sea surface temperatures: a global reconstruction, Mar. Micropaleontol., 27, 13–25, https://doi.org/10.1016/0377-8398(95)00050-X, 1996.

Duprat, L. P., Bigg, G. R., and Wilton, D. J.: Enhanced Southern Ocean marine productivity due to fertilization by giant icebergs, Nat. Geosci., 9, 219–221, https://doi.org/10.1038/ngeo2633, 2016.

Gerringa, L. J. A., Alderkamp, A.-C., Laan, P., Thuróczy, C.-E., De Baar, H. J. W., Mills, M. M., Van Dijken, G. L., Van Haren, H., and Arrigo, K. R.: Iron from melting glaciers fuels the phytoplankton blooms in Amundsen Sea (Southern Ocean): Iron biogeochemistry, Deep-Sea Res. Pt. II, 71–76, 16–31, https://doi.org/10.1016/j.dsr2.2012.03.007, 2012.

Greene, C. A., Gardner, A. S., Schlegel, N. J., and Fraser, A. D.: Antarctic calving loss rivals ice-shelf thinning, Nature, 609, 948–953, https://doi.org/10.1038/s41586-022-05037-w, 2022.

Grigorov, I., Pearce, R. B., and Kemp, A. E.: Southern Ocean laminated diatom ooze: mat deposits and potential for palaeo-flux studies, ODP leg 177, Site 1093, Deep-Sea Res. Pt. II, 49, 3391–3407, https://doi.org/10.1016/S0967-0645(02)00089-9, 2002.

Gohl, K., Wellner, J. S., Klaus, A., and the Expedition 379 Scientists: Expedition 379 Preliminary Report: Amundsen Sea West Antarctica Ice Sheet History, International Ocean Discovery Program, https://doi.org/10.14379/iodp.pr.379.2019, 2019.

Gohl, K., Wellner, J. S., Klaus, A., and the Expedition 379 Scientists: Amundsen Sea West Antarctic Ice Sheet History, Proceedings of the IODP 379, https://doi.org/10.14379/iodp.proc.379.2021, 2021.

Hillenbrand, C. D., Kuhn, G., and Frederichs, T.: Record of a Mid-Pleistocene depositional anomaly in West Antarctic continental margin sediments: an indicator for ice-sheet collapse?, Quaternary Sci. Rev., 28, 1147–1159, https://doi.org/10.1016/j.quascirev.2008.12.010, 2009.

Hopwood, M. J., Carroll, D., Höfer, J., Achterberg, E. P., Meire, L., Le Moigne, F. A., Bach, L. T., Eich, C., Sutherland, D. A., and González, H. E.: Highly variable iron content modulates iceberg-ocean fertilisation and potential carbon export, Nat. Commun., 10, 5261, https://doi.org/10.1038/s41467-019-13231-0, 2019.

Horrocks, J.: The formation and Late Quaternary palaeoenvironmental history of sediment mounds in the Amundsen Sea, West Antarctica, Doctoral dissertation, Durham University, https://nora.nerc.ac.uk/id/eprint/520455 (last access: 29 July 2024), 2018.

Johnson, T. C.: The dissolution of siliceous microfossils in surface sediments of the eastern tropical Pacific, Deep-Sea Res., 21, 851–864, https://doi.org/10.1016/0011-7471(74)90004-7, 1974.

Kemp, A. E., Pike, J., Pearce, R. B., and Lange, C. B.: The "Fall dump" – a new perspective on the role of a "shade flora" in the annual cycle of diatom production and export flux, Deep-Sea Res. Pt. II, 47, 2129–2154, https://doi.org/10.1016/S0967-0645(00)00019-9, 2000.

Kemp, A. E., Pearce, R. B., Grigorov, I., Rance, J., Lange, C. B., Quilty, P., and Salter, I.: Production of giant marine diatoms and their export at oceanic frontal zones: Implications for Si and C flux from stratified oceans, Global Biogeochem. Cy., 20, GB4S04, https://doi.org/10.1029/2006GB002698, 2006.

Kemp, A. E. S., Baldauf, J. G., and Pearce, R. B.: Origins and palaeoceanographic significance of laminated diatom ooze from the Eastern Equatorial Pacific Ocean, Geol. Soc. Lond. Spec. Publ., 116, 243–252, https://doi.org/10.1144/GSL.SP.1996.116.01.19, 1996.

Kemp, A. E. S., Grigorov, I., Pearce, R. B., and Garabato, A. N.: Migration of the Antarctic Polar Front through the mid-Pleistocene transition: evidence and climatic implications, Quaternary Sci. Rev., 29, 1993–2009, https://doi.org/10.1016/j.quascirev.2010.04.027, 2010.

Konfirst, M. A., Scherer, R. P., Hillenbrand, C. D., and Kuhn, G.: A marine diatom record from the Amundsen Sea – Insights into oceanographic and climatic response to the Mid-Pleistocene Transition in the West Antarctic sector of the Southern Ocean, Mar. Micropaleontol., 92, 40–51, https://doi.org/10.1016/j.marmicro.2012.05.001, 2012.

Kopczyńska, E., Fiala, M., and Jeandel, C.: Annual and interannual variability in phytoplankton at a permanent station off Kerguelen Islands, Southern Ocean, Polar Biol., 20, 342–351, https://doi.org/10.1007/s003000050312, 1998.

Lan, X., Hall, B. D., Dutton, G., Mühle, J., and Elkins, J. W.: Atmospheric composition, State of the Climate in 2018, Chapter 2: Global Climate, Special Online Supplement to the Bulletin of the American Met. Soc., Vol. 101, No. 8, https://doi.org/10.1175/2021BAMSStateoftheClimate.1, 2020.

Lin, H., Rauschenberg, S., Hexel, C. R., Shaw, T. J., and Twining, B. S.: Free-drifting icebergs as sources of iron to the Weddell Sea, Deep-Sea Res. Pt. II, 58, 1392–1406, https://doi.org/10.1016/j.dsr2.2010.11.020, 2011.

Laufkötter, C., Stern, A. A., John, J. G., Stock, C. A., and Dunne, J. P.: Glacial iron sources stimulate the southern ocean carbon cycle, Geophys. Res. Lett., 45, 13–377, https://doi.org/10.1029/2018GL079797, 2018.

Leventer, A.: Sediment trap diatom assemblages from the northern Antarctic Peninsula region, Deep-Sea Res. Pt. A, 38, 1127–1143, https://doi.org/10.1016/0198-0149(91)90099-2, 1991.

Leventer, A., Domack, E., Barkoukis, A., McAndrews, B., and Murray, J.: Laminations from the Palmer Deep: A diatom-based interpretation, Palaeoceanography, 17, PAL 3-1–PAL 3-15, https://doi.org/10.1029/2001PA000624, 2002.

Liguori, B. T., Almeida, M. G., and Rezende, C. E.: Barium and its Importance as an Indicator of (Paleo) Productivity, An. Acad. Bras. Ciênc., 88, 2093–2103, https://doi.org/10.1590/0001-3765201620140592, 2016.

McKay, R., Naish, T., Powell, R., Barrett, P., Scherer, R., Talarico, F., Kyle, P., Monien, D., Kuhn, G., Jackolski, C., and Williams, T.: Pleistocene variability of Antarctic Ice Sheet extent in the Ross Embayment, Quaternary Sci. Rev., 34, 93–112, https://doi.org/10.1016/j.quascirev.2011.12.012, 2012.

McMinn, A.: Comparison of Diatom Preservation Between Oxic and Anoxic Basins in Ellis Fjord Antarctica, Diatom Res., 10, 145–151, https://doi.org/10.1080/0269249X.1995.9705333, 1995.

Mercer, J. H.: West Antarctica Ice Sheet and CO_2 Greenhouse Effect: A Threat of Disaster, Nature, 271, 321–325, https://doi.org/10.1038/271321a0, 1978.

Morlighem, M., Rignot, E., Binder, T., Blankenship, D., Drews, R., Eagles, G., Eisen, O., Ferraccioli, F., and Forsberg, R., Fretwell, P., and Goel, V.: Deep glacial troughs and stabilizing ridges unveiled beneath the margins of the Antarctic ice sheet, Nat. Geosci., 13, 132–137, https://doi.org/10.1038/s41561-019-0510-8, 2020.

Mortlock, R. A. and Froelich, P. N.: A simple method for the rapid determination of biogenic opal in pelagic marine sediments, Deep-Sea Res. Pt. A., 36, 1415–1426, https://doi.org/10.1016/0198-0149(89)90092-7, 1989.

Naish, T., Powell, R., Levy, R., Wilson, G., Scherer, R., Talarico, F., Krissek, L., Niessen, F., Pompilio, M., Wilson, T., and Carter, L.: Obliquity-paced Pliocene West Antarctic ice sheet oscillations, Nature, 458, 322–328, https://doi.org/10.1038/nature07867, 2009.

Paytan, A. and Griffith, E. M.: Marine barite: Recorder of variations in ocean export Productivity, Deep-Sea Res. Pt. II, 54, 687–705, https://doi.org/10.1016/j.dsr2.2007.01.007, 2007.

Planquette, H., Sherrell, R. M., Stammerjohn, S., and Field, M. P.: Particulate iron delivery to the water column of the Amundsen Sea, Antarctica, Mar. Chem., 153, 15–30, https://doi.org/10.1016/j.marchem.2013.04.006, 2013.

Pollard, D. and DeConto, R.: Modelling West Antarctic ice sheet growth and collapse through the past five million years, Nature, 458, 329–332, https://doi.org/10.1038/nature07809, 2009.

Pollock, D. E.: The role of diatoms, dissolved silicate and Antarctic glaciation in glacial/interglacial climatic change: a hypothesis, Global Planet. Change, 14, 113–125, https://doi.org/10.1016/S0921-8181(96)00005-7, 1997.

Quilty, P. G., Kerry, K. R., and Marchant, H. J.: A seasonally recurrent patch of Antarctic planktonic diatoms, Search, 16, 48–51, 1985.

Raiswell, R., Benning, L. G., Tranter, M., and Tulaczyk, S.: Bioavailable iron in the Southern Ocean: the significance of the iceberg conveyor belt, Geochem. T., 9, 1–9, https://doi.org/10.1186/1467-4866-9-7, 2008.

Raiswell, R., Hawkings, J. R., Benning, L. G., Baker, A. R., Death, R., Albani, S., Mahowald, N., Krom, M. D., Poulton, S. W., Wadham, J., and Tranter, M.: Potentially bioavailable iron delivery by iceberg-hosted sediments and atmospheric dust to the polar oceans, Biogeosciences, 13, 3887–3900, https://doi.org/10.5194/bg-13-3887-2016, 2016.

Rignot, E., Mouginot, J., Scheuchl, B., Van Den Broeke, M., Van Wessem, M. J., and Morlighem, M.: Four decades of Antarctic Ice Sheet mass balance from 1979–2017, P. Natl. Acad. Sci., 116, 1095–1103, https://doi.org/10.1073/pnas.1812883116, 2019.

Robinson, D. E., Menzies, J., Wellner, J. S., and Clark, R. W.: Subglacial sediment deformation in the Ross Sea, Antarctica, Quaternary Sci. Adv., 4, 100029, https://doi.org/10.1016/j.qsa.2021.100029, 2021.

Ruggiero, J. A., Scherer, R. P., Mastro, J., Lopez, C., Angus, M., Unger-Harquail, E., Quartz, O., Leventer, A., and Hillenbrand,

C.-D.: Last Interglacial Southern Ocean paleothermometry from diatom morphometrics: Analysis and application of the *F. kerguelensis* valve rectangularity sea surface temperature proxy, J. Micropalaeontol., in press, 2024.

Scherer, R. P.: Pliocene diatom abundance, IODP 397-U1532, USAP-DC [data set], https://www.usap-dc.org/view/dataset/601769, last access: 20 February 2024.

Scherer, R. P., Aldahan, A., Tulaczyk, S., Possnert, G., Engelhardt, H., and Kamb, B.: Pleistocene Collapse of the West Antarctic Ice Sheet, Science, 281, 82–85, https://doi.org/10.1126/science.281.5373.82, 1998.

Smith Jr., K. L., Robison, B. H., Helly, J. J., Kaufmann, R. S., Ruhl, H. A., Shaw, T. J., Twining, B. S., and Vernet, M.: Free-drifting icebergs: hot spots of chemical and biological enrichment in the Weddell Sea, Science, 317, 478–482, https://doi.org/10.1126/science.1142834, 2007.

Stephenson Jr., G. R., Sprintall, J., Gille, S. T., Vernet, M., Helly, J. J., and Kaufmann, R. S.: Subsurface melting of a free-floating Antarctic iceberg, Deep-Sea Res. Pt. II, 58, 1336–1345, https://doi.org/10.1016/j.dsr2.2010.11.009, 2011.

St-Laurent, P., Yager, P. L., Sherrell, R. M., Stammerjohn, S. E., and Dinniman, M. S.: Pathways and supply of dissolved iron in the Amundsen Sea (Antarctica), J. Geophys. Res.-Oceans, 122, 7135–7162, https://doi.org/10.1002/2017JC013162, 2017.

St-Laurent, P., Yager, P. L., Sherrell, R. M., Oliver, H., Dinniman, M. S., and Stammerjohn, S. E.: Modeling the seasonal cycle of iron and carbon fluxes in the Amundsen Sea Polynya, Antarctica, J. Geophys. Res.-Oceans, 124, 1544–1565, https://doi.org/10.1029/2018JC014773, 2019.

Thuróczy, C.-E., Alderkamp, A.-C., Laan, P., Gerringa, L. J. A., Mills, M. M., Van Dijken, G. L., De Baar, H. J. W., and Arrigo, K. R.: Key role of organic complexation of iron in sustaining phytoplankton blooms in the Pine Island and Amundsen Polynyas (Southern Ocean), Deep-Sea Res. Pt. II, 71–76, 49–60, https://doi.org/10.1016/j.dsr2.2012.03.009, 2012.

Warnock, J. P. and Scherer, R. P.: A revised method for determining the absolute abundance of diatoms, Paleolimnol., 53, 157–163, https://doi.org/10.1007/s10933-014-9808-0, 2015a.

Warnock, J. P. and Scherer, R. P.: Diatom species abundance and morphologically-based dissolution proxies in coastal Southern Ocean assemblages, Cont. Shelf Res., 102, 1–8, https://doi.org/10.1016/j.csr.2015.04.012, 2015b.

Wu, S.-Y. and Hou, S.: Impact of icebergs on net primary productivity in the Southern Ocean, The Cryosphere, 11, 707–722, https://doi.org/10.5194/tc-11-707-2017, 2017.

Zielinski, U. and Gersonde, R.: Diatom distribution in Southern Ocean surface sediments (Atlantic sector): Implications for paleoenvironmental reconstructions, Palaeogeogr. Palaeoecol., 129, 213–250, https://doi.org/10.1016/S0031-0182(96)00130-7, 1997.

Zielinski, U., Bianchi, C., Gersonde, R., and Kunz-Pirrung, M.: Last occurrence datums of the diatoms Rouxia leventerae and Rouxia constricta: indicators for marine isotope stages 6 and 8 in Southern Ocean sediments, Mar. Micropaleontol., 46, 127–137, https://doi.org/10.1016/S0377-8398(02)00042-7, 2002.